

Stable water isotopologue fractionation during soil-water evaporation: Analysis using a coupled soil-atmosphere model

Stefanie Kiemle¹, Katharina Heck¹, Edward Coltman¹, and Rainer Helmig¹

¹University of Stuttgart

November 28, 2022

Abstract

Stable water isotopologues tend to fractionate from ordinary water during evaporation processes resulting in an enrichment of the isotopic species in the soil. The fractionation process can be split into equilibrium fractionation and kinetic fractionation. Due to the complex coupled processes involved in simulating soil-water evaporation accurately, defining the kinetic fractionation correctly remains an open research area. In this work, we present a multi-phase multi-component transport model that resolves flow through both the near surface atmosphere and the soil, and models transport and fractionation of the stable water isotopologues using the numerical simulation environment DuMuX. Using this high resolution coupled model, we simulate transport and fractionation processes of stable water isotopologues in soils and the atmosphere without further parameterization of the kinetic fractionation process as is commonly done. In a series of examples, the transport and distribution of stable-water isotopologues are evaluated numerically with varied conditions and assumptions. First, an unsaturated porous medium connected to constant laminar flow conditions is introduced. The expected vertical isotope profiles in the soil as described in literature are reproduced. Further, by examining the spatial and temporal distribution of the isotopic composition, is determined the enrichment of the isotopologues in soil is linked with the different stages of the evaporation process. Building on these results, the robustness of the isotopic fractionation in our model is analysed by isolating single fractionation parameters. The effect of wind velocity and turbulent atmospheric conditions is investigated, leading to different kinetic fractionation scenarios and varied isotopic compositions in the soil.

1 **Stable water isotopologue fractionation during**
2 **soil-water evaporation: Analysis using a coupled**
3 **soil-atmosphere model**

4 **Stefanie Kiemle¹, Katharina Heck¹, Edward Coltman¹, Rainer Helmig¹**

5 ¹Institute for Modelling Hydraulic and Environmental Systems, Department of Hydromechanics and
6 Modelling of Hydrosystems, University of Stuttgart, Stuttgart, Germany

7 **Key Points:**

- 8 • Stable water isotopologue distribution in the unsaturated zone
9 • Coupled soil-atmosphere models
10 • Isotopic fractionation processes during evaporation

Corresponding author: Stefanie Kiemle, stefanie.kiemle@iws.uni-stuttgart.de

Abstract

[Stable water isotopologues tend to fractionate from ordinary water during evaporation processes resulting in an enrichment of the isotopic species in the soil. The fractionation process can be split into equilibrium fractionation and kinetic fractionation. Due to the complex coupled processes involved in simulating soil-water evaporation accurately, defining the kinetic fractionation correctly remains an open research area. In this work, we present a multi-phase multi-component transport model that resolves flow through both the near surface atmosphere and the soil, and models transport and fractionation of the stable water isotopologues using the numerical simulation environment DuMu^x. Using this high resolution coupled model, we simulate transport and fractionation processes of stable water isotopologues in soils and the atmosphere without further parameterization of the kinetic fractionation process as is commonly done.

In a series of examples, the transport and distribution of stable-water isotopologues are evaluated numerically with varied conditions and assumptions. First, an unsaturated porous medium connected to constant laminar flow conditions is introduced. The expected vertical isotope profiles in the soil as described in literature are reproduced. Further, by examining the spatial and temporal distribution of the isotopic composition, is determined the enrichment of the isotopologues in soil is linked with the different stages of the evaporation process. Building on these results, the robustness of the isotopic fractionation in our model is analysed by isolating single fractionation parameters. The effect of wind velocity and turbulent atmospheric conditions is investigated, leading to different kinetic fractionation scenarios and varied isotopic compositions in the soil.

]

1 Introduction

Stable water isotopologues are commonly used as natural tracers to determine the water movement within the unsaturated zone (e.g. Sprenger et al., 2016, 2018). Analyzing their compositions in water has proven to be a suitable tool for better understanding evaporation and mixing processes within soils and at the soil-atmosphere interface. For instance, the location of the evaporation front within the soil can be identified by measuring the isotopic composition (Rothfuss et al., 2015). During evaporation, stable water isotopologues are affected by fractionation processes. In soil-atmosphere systems this process can be divided into equilibrium and kinetic fractionation (Craig, 1961; Craig & Gordon, 1965). Due to their differences in vapor pressure (equilibrium fractionation) and their varied diffusion coefficients (kinetic fractionation), the transport and flow behavior of stable water isotopologues is different in comparison to ordinary water.

Whereas the description of the equilibrium fractionation is consistent in literature (Majoube, 1971; Horita & Wesolowski, 1994; Luz et al., 2009), in terms of the kinetic fractionation, there are uncertainties in defining the relationship between the vapor diffusion coefficients under evaporating conditions (e.g. Quade et al., 2018; Luz et al., 2009). The major challenge in determining the kinetic fractionation correctly is how to include the influence of the atmosphere under different wind velocities (Quade et al., 2018).

In the past, many one-dimensional process-based models have been developed: ODWISH (Shurbaji & Phillips, 1995), MOISE (Mathieu & Bariac, 1996; Melayah et al., 1996), SiSPAT-Isotope (Braud et al., 2005), Soil-Litter-Iso (Haverd & Cuntz, 2010), HYDRUS isotope module (Stumpp et al., 2012), SWIS (Müller et al., 2014; Sprenger et al., 2018), HYDRUS-1D (Zhou et al., 2021). With these 1D model approaches, fractionation processes within the unsaturated zone and in the interface region can be simulated. However, these models only cover the influence of the free-flow domain by including evaporation boundary conditions and using parameterizations to describe the kinetic fractionation. Thus, the influence of the free flow on the fractionation process can only be modeled for certain conditions where suitable parameterizations are available. Additionally, the spatial dis-

62 tribution of the isotopologues is only analyzed in 1D, and possible multidimensional ef-
63 fects cannot be analyzed with these models.

64 Concerning multi-dimensional isotopologue transport models in the subsurface, some
65 models can be found in literature: TAC^D (Uhlenbrook et al., 2004), NASA-Giss Mod-
66 elleE (Aleinov & Schmidt, 2006), CMF (Kraft et al., 2011; Windhorst et al., 2014), ECHAM5-
67 JSBACH-wiso (Haese et al., 2012), ORCHIDEE (Risi et al., 2016), iCLM4 (Wong et al.,
68 2017), EcoH2O-iso* (Kuppel et al., 2018), TOUGH2 (Jiang et al., 2018). However, be-
69 sides the issue that these models operate on a larger scale with lower resolution (land
70 surface or catchment models) than our target scale, they also rely on parameterizations
71 to describe the isotope transport and fractionation. Further, none of these models in-
72 clude the influence of atmospheric flow on the isotopic fractionation processes in the porous-
73 medium domain by accounting for the flow and transport in the free-flow domain and
74 coupling the free-flow to the porous-medium domain. To our knowledge, there is no sta-
75 ble water isotopologue transport model, which resolves both domains and couples the
76 free-flow and the porous-medium domain.

77 In the following, we present a multi-dimensional stable water isotopologue trans-
78 port model which couples a free-flow domain and a porous-medium domain and ensures
79 mass, momentum, and energy conservation. Evaporation of both ordinary water and iso-
80 topologues can be described under varying free-flow conditions, e.g., varying wind speeds
81 including turbulent and laminar flow conditions. This means we can describe the frac-
82 tionation process in the free-flow domain, the interface region, and the porous-medium
83 domain without implementing the commonly used fractionation parameterizations. This
84 allows us to analyze the flow and transport of the isotopologues together with the evap-
85 oration process of ordinary water. Further, the influence of the different stages of the evap-
86 oration processes on isotopologue behavior can be reviewed. It also allows us to isolate
87 physical factors, analyzing the processes contributing to isotopologue fractionation in-
88 dependently.

89 2 Methods

90 In this section, we describe the principles of fractionation processes of stable wa-
91 ter isotopologues during evaporation from soils (Section 2.1), as well as the applied cou-
92 pled model concept (Section 2.2). This model concept includes the description of mass
93 and energy transfer within the porous-medium domain Ω_{pm} , within the atmospheric free-
94 flow domain Ω_{ff} , and the coupling concept connecting the domains. At the end of the
95 chapter, the numerical model is briefly explained in Section 2.3.

96 2.1 Fractionation Processes of Stable Water Isotopologues

97 Craig and Gordon (1965) proposed a model for isotopic effects during evaporation
98 from a free water surface. The so-called Craig-Gordon model describes the effects of the
99 different transport mechanisms and fractionation processes between the water surface
100 and the ambient air.

101 The original Craig-Gordon model is distributed into three zones. These zones can
102 be adapted for the application in porous medium by extending the zones to the soil-water
103 evaporation front. These zones are as follows: (1) a turbulent zone where turbulent mix-
104 ing occurs and the isotopic composition becomes constant; (2) a diffusive zone defined
105 by the viscous sub-layer where diffusive transport dominates and kinetic fractionation
106 is the leading fractionation process; and (3) an interface zone where the liquid and va-
107 por phase are in isotopic equilibrium inside the porous medium and equilibrium fraction-
108 ation governs the fractionation process. In Figure 1, the isotopic composition profile and
109 the classification into the specific fractionation zone are illustrated.

110 Analyzing the enrichment of isotopic species in soils can be used to determine the
 111 depth or progression of the evaporation front in unsaturated soils. The evaporation front
 112 can be located at the maximal gradient of the isotopic composition (Rothfuss et al., 2015).
 113 This and the impact of the different evaporation stages on the enrichment process are
 114 depicted in Figure 1.

115 During stage-I evaporation (Figure 1a), the the atmospheric evaporation potential
 116 is satisfied at the soil-atmosphere interface by capillary recharge. As the soil dries out
 117 further, the evaporation rate reduces as stage-II evaporation begins (Figure 1b) (e.g. Lehmann
 118 et al., 2008). Here, liquid water at the interface is no longer mobile and evaporation is
 119 possible through diffusive transport. While the soil dries out, the position of the isotopic
 120 zones rearranges. The interface zone, characterized by equilibrium fractionation, moves
 121 with the evaporation front downwards, and the diffusive zone, characterized by kinetic
 122 fractionation, is thereby extended. The maximal gradient of the isotopic composition and
 123 so the evaporation front is no longer located at the porous-medium domain surface, but
 below the soil surface, in the transition between the diffusive and interface zone.

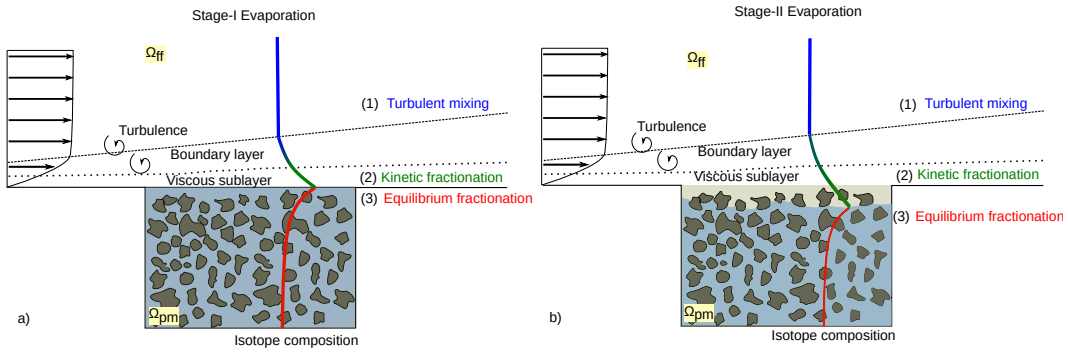


Figure 1: Isotopic composition profiles during (a) stage-I evaporation, (b) stage-II evaporation and the classification into their respective isotopic fractionation processes.

124

125 The main driving processes for isotopic fractionation in soils and at the soil-atmosphere
 126 interface are commonly expressed by the equilibrium fractionation factor and the kinetic
 127 fractionation factor. These factors are normally expressed by the symbol α . However,
 128 to avoid misunderstandings with the definition of the subscripts α describing the phases,
 129 we denote the fractionation factors in the following with β . In general, the fractionation
 130 factor describes the tendency of two components κ to separate from its mixture.

131 The isotopic equilibrium fractionation factor β_{eq}^i describes the phase equilibrium
 132 between liquid and gaseous phases for water and its isotopologues (Majoube, 1971; Van Hook,
 133 1968),

$$\frac{x_l^i}{x_l^{H_2O}} \beta_{eq}^i = \frac{x_g^i}{x_g^{H_2O}}, \quad (1)$$

134 with x denoting the mole fraction of a component $\kappa \in \{i, H_2O\}$. Here, the i stands
 135 for the heavier isotopologues while H_2O denotes ordinary water. Phase indices are de-
 136 noted by the subscript α in general and specifically with l for the liquid phase and g for
 137 the gaseous phase.

The equilibrium fractionation factor is defined by the different vapor pressures of
 the isotopologues p_g^i and ordinary water $p_g^{H_2O}$ and is commonly expressed by the depen-

dence on the temperature T and coefficients that can be chosen from literature:

$$\beta_{eq}^i = \frac{p_g^i}{p_{H_2O}^i} = \exp\left(-\left(\frac{A}{T^2} + \frac{B}{T} + C\right)\right). \quad (2)$$

138 With this definition, the equilibrium fractionation factor is smaller than 1, which
 139 leads to the enrichment of the isotopologues in liquid water compared to ordinary wa-
 140 ter. More information about the used coefficients can be found in Section 3.

141 For the kinetic fractionation factor, which describes the fractionation of isotopic
 142 species caused by the difference in diffusive transport of water and its isotopologues, many
 143 approaches exists. Barnes and Allison (1984) described the kinetic fractionation factor
 144 considering only molecular transport. Dongmann et al. (1974) (see Eq. 3) extended the
 145 definition of Barnes and Allison (1984) by involving free-flow properties. Besides these
 146 definitions Brutsaert (1975), Mathieu and Bariac (1996), Gat (1971), Craig and Gordon
 147 (1965), Quade et al. (2018) published alternative formulations. The kinetic fractiona-
 148 tion factor is commonly described by the diffusion coefficients D :

$$\beta_{kin}^i = \left(\frac{D_{H_2O}^i}{D_g^i}\right)^n. \quad (3)$$

149 In the above-described literature, the exponent n varies depending on the free-flow
 150 conditions (turbulent or laminar). However, the fully resolved coupled model does not
 151 use a kinetic fractionation factor. This factor is implicitly included in the model via their
 152 different diffusion coefficients used in the transport equations in both the free-flow and
 153 the porous-medium domains. In Section 3, details about the diffusion coefficients used
 154 can be found.

155 In the coupled model, equilibrium and diffusive fractionation effects are described
 156 by solving two-phase four-component transport equations in the porous medium and one-
 157 phase four-component transport equations in the free-flow domain. Both domains are
 158 coupled with the help of suitable coupling conditions that ensure mass, momentum, and
 159 energy conservation.

160 In the following model concepts for the porous-medium domain, the free-flow do-
 161 main, and the coupling conditions are presented.

162 **2.2 Coupled Model Concepts**

163 *Porous-Medium Domain*

164 The porous-medium flow domain is described by a multiphase Darcy's law in com-
 165 bination with a mass and energy balance to describe non-isothermal, multiphase flow.
 166 The mass balance equation for the component transport is written as the following:

$$\sum_{\alpha \in \{l, g\}} \left(\phi \frac{\partial (\rho_\alpha S_\alpha X_\alpha^\kappa)}{\partial t} + \nabla \cdot \mathbf{v}_\alpha \rho_\alpha X_\alpha^\kappa + \sum_{\kappa} \nabla \cdot (\mathbf{D}_{pm, \alpha}^\kappa \rho_\alpha \nabla X_\alpha^\kappa) \right) = 0, \quad (4)$$

167 here $\mathbf{D}_{pm, \alpha}^\kappa$ denotes the effective binary diffusion coefficient in the porous medium.
 168 Phase saturations are denoted by S_α and ρ_α is the density of the phase. X_α^κ is the mass
 169 fraction that is defined by $X_\alpha^\kappa = x_\alpha^\kappa \frac{M^\kappa}{M_\alpha}$ with M^κ as the molar mass of the component
 170 and M_α as the average molar mass of the phase. The fluid phase velocity \mathbf{v}_α is deter-
 171 mined by Eq. 5:

$$\mathbf{v}_\alpha = -\frac{k_{r,\alpha}}{\mu_\alpha} K (\nabla p_\alpha - \rho_\alpha \mathbf{g}). \quad (5)$$

K denotes the intrinsic permeability of the porous medium and $k_{r,\alpha}$ the relative permeability of the phase. μ_α is the dynamic viscosity of the phase. Gravity is denoted by the vector \mathbf{g} . Within the porous-medium domain we assume a local thermodynamic equilibrium. The energy balance is defined by:

$$\sum_{\alpha \in \{l, g\}} \left(\phi \frac{\partial (\rho_\alpha S_\alpha u_\alpha)}{\partial t} + \nabla \cdot (\rho_\alpha h_\alpha \mathbf{v}_\alpha) \right) + (1 - \phi) \frac{\partial (\rho_s c_{p,s} T)}{\partial t} - \nabla \cdot (\lambda_{pm} \nabla T) = 0. \quad (6)$$

172 u_α is the internal energy of the phase and h_α the specific enthalpy. Due to the differ-
 173 ences in enthalpies of the gaseous and the liquid phase, latent heat of vaporization is
 174 included in this approach. The solid part of the porous medium is accounted for by the
 175 specific heat capacity $c_{p,s}$ and the density of the solid ρ_s . The thermal conductivity λ_{pm}
 176 is a mixture of the thermal conductivities of the liquid and the gaseous and the solid phase
 177 and is computed by the Somerton approach (Somerton et al., 1974).

178 *Free-Flow Domain*

The free flow can be described by the Navier-Stokes equations:

$$\frac{\partial \rho_g \mathbf{v}_g}{\partial t} + \nabla \cdot (\rho_g \mathbf{v}_g \mathbf{v}_g^T) - \nabla \cdot (\boldsymbol{\tau}_g) + \nabla \cdot (p_g \mathbf{I}) - \rho_g \mathbf{g} = 0. \quad (7)$$

with \mathbf{I} as the identity matrix. The mass balance for each component is given by:

$$\frac{\partial (\rho_g X_g^\kappa)}{\partial t} + \nabla \cdot (\rho_g \mathbf{v}_g X_g^\kappa - \mathbf{j}_{\text{diff}}^\kappa) - q^\kappa = 0. \quad (8)$$

179 The diffusive fluxes $\mathbf{j}_{\text{diff}}^\kappa = \mathbf{D}_\alpha^\kappa \rho_\alpha \nabla X_\alpha^\kappa$ are, as in the porous medium, described by Fick's
 180 law.

181 In order to properly describe turbulent free-flow behaviour the so-called Reynolds-
 182 Averaged Navier-Stokes (RANS) equations are used. This splits the fluctuating terms
 183 into averaged and fluctuating values, which introduces a new term, the Reynolds stress
 184 tensor $\boldsymbol{\tau}_{g,t}$. The momentum balance then can be denoted as:

$$\frac{\partial \rho_g \mathbf{v}_g}{\partial t} + \nabla \cdot (\rho_g \mathbf{v}_g \mathbf{v}_g^T) - \nabla \cdot (\boldsymbol{\tau}_g + \boldsymbol{\tau}_{g,t}) + \nabla \cdot (p_g \mathbf{I}) - \rho_g \mathbf{g} = 0. \quad (9)$$

185 As closure relations for the newly introduced Reynold's stress $\boldsymbol{\tau}_{g,t} = \mu_{g,t} (\nabla \mathbf{v}_g +$
 186 $\nabla \mathbf{v}_g^T) - (\frac{2}{3} \rho_g k \mathbf{I})$ in this work a $k-\omega$ turbulence model is used. More information about
 187 this can be found in Wilcox (2008).

The mass balance equation for the transport of a component in the free flow is given
 with:

$$\frac{\partial (\rho_g X_g^\kappa)}{\partial t} + \nabla \cdot (\rho_g \mathbf{v}_g X_g^\kappa - \mathbf{j}_{\text{diff},t}^\kappa) - q^\kappa = 0. \quad (10)$$

188 where the turbulent diffusion $\mathbf{j}_{\text{diff},t}^\kappa$ uses an effective diffusion coefficient that also accounts
 189 for turbulent behaviour with: $D_{\text{eff},t}^{ij} = D_g^{ij} + D_t$. D_t is the eddy diffusivity.

The energy balance can be described with:

$$\frac{\partial (\rho_g u_g)}{\partial t} + \nabla \cdot (\rho_g h_g \mathbf{v}_g) + \sum_i \nabla \cdot (h_g \mathbf{j}_{\text{diff},t}^\kappa) - \nabla \cdot ((\lambda_g + \lambda_t) \nabla T) = 0, \quad (11)$$

190 where the λ_t is the eddy conductivity. More information about these models can be found
 191 in e.g. Fetzler et al. (2016).

192

Interface Coupling Conditions

193

194

195

196

The interface conditions are based on the assumption of local thermodynamic equilibrium (Mosthaf et al., 2011). At the interface we assume that temperatures, the pressure and mole fractions are equal. Continuity of fluxes at the interface is then described by:

$$[(\rho_g \mathbf{v}_g) \cdot \mathbf{n}]^{\text{ff}} = -[(\rho_g \mathbf{v}_g + \rho_w \mathbf{v}_w) \cdot \mathbf{n}]^{\text{pm}}. \quad (12)$$

The tangential component of the momentum balance is set to the Beavers-Joseph-Saffman condition (Beavers & Joseph, 1967; Saffman, 1971; Jones, 1973), describing the slip velocity at the interface.

$$\left[\left(-\mathbf{v}_g - \frac{\sqrt{(\mathbf{K} \mathbf{t}_i) \cdot \mathbf{t}_i}}{\alpha_{BJ}} (\nabla \mathbf{v}_g + \nabla \mathbf{v}_g^T) \mathbf{n} \right) \cdot \mathbf{t}_i \right]^{\text{ff}} = 0, \quad i \in \{1, \dots, d-1\}. \quad (13)$$

197

198

For the normal part of the momentum coupling condition, we use a continuity of normal stresses.

$$[(\rho_g \mathbf{v}_g \mathbf{v}_g^T - (\boldsymbol{\tau}_g + \boldsymbol{\tau}_{g,t}) + p_g \mathbf{I}) \mathbf{n}]^{\text{ff}} = [(p_g \mathbf{I}) \mathbf{n}]^{\text{pm}}. \quad (14)$$

For a component, i , continuity of fluxes is written as:

$$[(\rho_g X_g^\kappa \mathbf{v}_g + \mathbf{j}_{\text{diff},t}) \cdot \mathbf{n}]^{\text{ff}} = - \left[\left(\sum_{\alpha} (\rho_{\alpha} X_{\alpha}^{\kappa} \mathbf{v}_{\alpha} + \mathbf{j}_{\text{diff},\alpha}^{\kappa}) \right) \cdot \mathbf{n} \right]^{\text{pm}}. \quad (15)$$

For the energy coupling the flux condition is:

$$\left[\left(\rho_g h_g \mathbf{v}_g + \sum_i h_g^{\kappa} \mathbf{j}_{\text{diff},g}^{\kappa} + \lambda_g \nabla T \right) \cdot \mathbf{n} \right]^{\text{ff}} = - \left[\left(\sum_{\alpha} (\rho_{\alpha} h_{\alpha} \mathbf{v}_{\alpha} + \sum_i h_{\alpha}^{\kappa} \mathbf{j}_{\text{diff},\alpha}^{\kappa}) - \lambda_{\text{pm}} \nabla T \right) \cdot \mathbf{n} \right]^{\text{pm}}. \quad (16)$$

199

2.3 Numerical Model

200

201

202

203

The porous-medium domain is discretized using cell-centered finite volumes. The simulations were performed using a two-point flux approximation on a rectangular grid. The free-flow domain is also discretized using finite volumes but with the marker and cell scheme. More details are described in (Coltman et al., 2020).

204

205

206

207

The above-mentioned concepts are implemented using the open-source simulation environment DuMu^x (Koch et al., 2021; Flemisch et al., 2011), which is based on the open-source numerical toolbox DUNE. The source code for the below-performed simulations is accessible via a DuMu^x publication module (?, ?).

208

3 Simulation Scenario

209

210

211

In our analysis we investigated the fractionation behaviour of the heavy water isotopologues $^1H^2HO$ and $H_2^{18}O$ in relation to the lighter ordinary water H_2O during an evaporation process.

212

213

214

Therefore, we created a virtual evaporation case in which a partially-saturated soil column dries out under constant atmospheric conditions. The setup comprises a wind tunnel with a flat porous medium beneath. The wind velocity profile develops from the

215 left to the right side from a parabolic-shaped profile into a fully developed velocity pro-
 216 file. From the left side, the free-flow domain is constantly supplied with stable water iso-
 217 topologues and water vapor. Figure 2 shows a sketch for the initial and boundary con-
 218 ditions of the simulation setup. As this evaluation does not include any specific pore scale
 219 information, the Beavers-Joseph coefficient α_{BJ} , used in the tangential momentum cou-
 220 pling condition, is set to 1.

221 Inside the porous-medium domain, we used a light clay (Yolo light clay ((Moore,
 222 1937))) with a texture of 31.2 % clay, 45.0 % silt and 23.8 % sand for our simulations.
 223 The spatial parameters of the used soil are listed in Table 1.

224 The applied fluid system comprises the components *air*, H_2O , $^1H^2HO$ and $H_2^{18}O$.
 225 The non-isotopic properties and relationships of our fluid system can be found in (IAPWS,
 226 2007), as well as in the DuMu^x documentation and in the DuMu^x publication module
 227 (git.iws.uni-stuttgart.de/dumux-pub/Kiemle2022a). The binary liquid diffusion coeffi-
 228 cient for " H_2O - isotopologue" is proportional to the liquid self-diffusion coefficient of
 229 H_2O . The proportional factor can be found in Mathieu and Bariac (1996). The diffu-
 230 sion between air-isotopologues in the vapor phase was defined by using the gas diffusion
 231 coefficient of H_2O -Air and a proportional factor given by Merlivat (1978). The isotopic
 232 vapor pressure (see Eq. 2) was defined by using coefficients proposed by Van Hook (1968).

233 The composition of isotopologues is commonly written in the δ notation that re-
 234 lates the ratio of isotopologues to ordinary water to a standard value: $\delta_\alpha^i = \frac{R_\alpha^i - R_{V-SMOW}}{R_{V-SMOW}}$.
 235 $1000[\text{‰}]$ with $R_\alpha^i = \frac{N^i}{N^w}$ and R_{V-SMOW} the standard mean ocean water (Gonfiantini,
 236 1978). Concerning the δ -notation, the superscript i describes only the heavier atom of
 237 the isotopologue instead of the entire molecule.

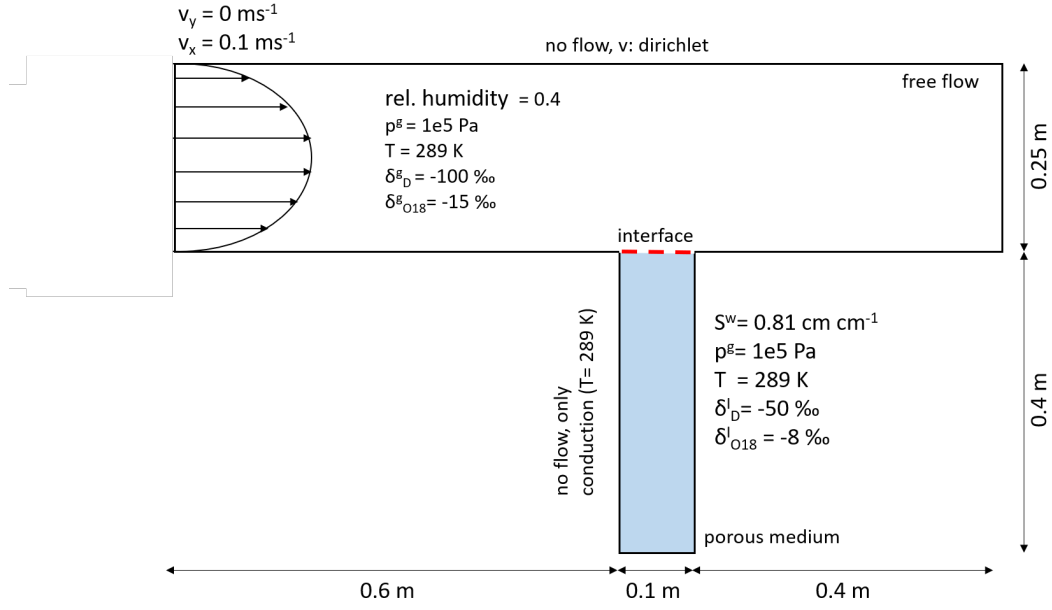


Figure 2: Initial and boundary conditions for analysing stable water isotopic fractionation during evaporation. The problem is discretized using 100 cells/m in the vertical direction and with 400 cells/m (porous-medium domain) and 100 cells/m (free-flow domain) in the horizontal direction. A vertical grid refinement towards the interface region is used.

Table 1: Spatial parameters of Yolo light clay

Parameter	Value
Porosity ϕ	0.35
Permeability K	1.23E-14 m ²
Residual saturation of non-wetting phase S_{nr}	0.00
Residual saturation of wetting phase S_{wr}	0.00
Van Genuchten parameter n	2.221
Van Genuchten parameter α	0.0005 Pa ⁻¹
Solid density ρ_s	1300 kg m ⁻³
Solid thermal conductivity λ_{pm}	0.5 W m ⁻¹ K ⁻¹
Solid heat capacity $c_{p,s}$	1300 J kg ⁻¹ K ⁻¹

238

4 Results and Discussion

239

240

In the following analysis, we set up a series of examples to investigate the transport and distribution of stable water isotopologues during the evaporation of the unsat-

241 urated porous medium. Using laminar flow conditions, we show that the spatial and tem-
 242 poral distribution of the isotopic composition match with the description in literature
 243 (Section 4.1), and by isolating single fractionation parameters, we highlight the robust-
 244 ness of our fractionation model (Section 4.2). Additionally, we present the variety of our
 245 coupled model by changing wind velocity and turbulent atmospheric conditions (Section
 246 4.3).

247 4.1 Water isotopologue transport under laminar flow conditions

248 We focus on the fractionation behaviour in the porous-medium domain during the
 249 evaporation of a soil column. As described in Section 2.1, we expect an enrichment of
 250 isotopologues towards the evaporation front in the porous-medium domain caused by the
 251 equilibrium fractionation factor in the saturated zone and subsequently a decrease in the
 252 isotopic composition caused by intrusion of the isotopic-depleted atmosphere in the dried
 253 porous-medium zone. Thus the resulting isotope profile remains constant in the satu-
 254 rated zone (no fractionation), but forms a peak-shape at the evaporation front.

255 As a first step, we set up a stable water isotopologue transport problem with lam-
 256 inar flow ($v_x = 0.1$ m/s) above the porous-medium domain. Here, focus is placed on the
 257 isotope fractionation process itself without the influence of turbulent mixing in the free
 258 flow. In Figure 3, the isotopic compositions for various days are plotted as (a) vertical
 259 and (b) horizontal profiles. In the vertical profiles, it can be observed that the simulated
 260 profiles match the theoretical description depicted in Figure 1. Both, the isotopic enrich-
 261 ment towards the evaporation front and the depletion in the dry domain of the porous
 262 medium are simulated. Further, we observe how the soil column dries out over time as
 263 the evaporation front propagates downwards.

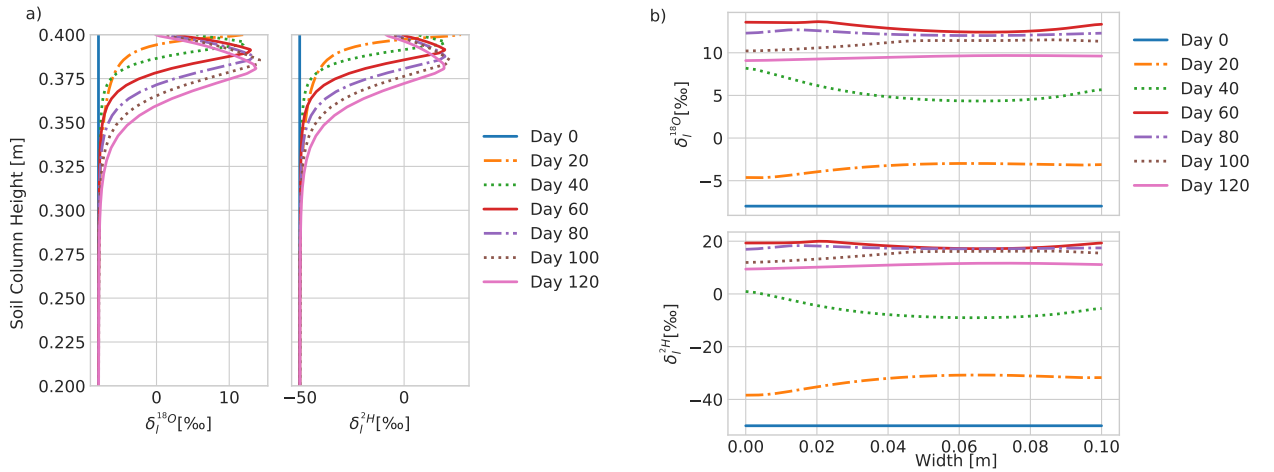


Figure 3: Isotopic composition δ_i^z over time. (a) Vertical relative concentration profile in the middle of the soil column at selected days; (b) horizontal relative concentration profile at 0.39 m soil column height at selected days.

264 In the horizontal profiles, the spatial distribution across the x-axis of the isotopo-
 265 logues and their fractionation behavior are visible. As the flow profile is developed from
 266 the left side and we consider conduction at all boundaries of the porous-medium domain,
 267 a spatial variation in isotopic composition can be observed. As seen in the vertical iso-
 268 topic profiles, the isotopic species are either enriched or depleted in the porous-medium

269 domain. During stage-I evaporation, the isotopologues enrich over the whole column width.
 270 As evaporation progresses, the upper layers of the porous-medium domain dries com-
 271 pletely, and the isotopologues are depleted because the influence of the atmosphere with
 272 low isotopic concentration increase.

273 In our study, we analyze how the different stages of evaporation influences the enrich-
 274 ment of the water isotopologues. In Figure 4, the temporal isotopic composition evo-
 275 lution for different soil column depths and the corresponding evaporation rate are plot-
 276 ted. We can see that during stage-I evaporation, where evaporation rates are higher, the
 277 isotopic composition first enriches before depletion. This enrichment peak is here referred
 278 to as "stage-I peak". Afterwards, during the transition to stage-II evaporation, we ob-
 279 serve another peak in isotopologue composition, which we refer to as "stage-II peak".

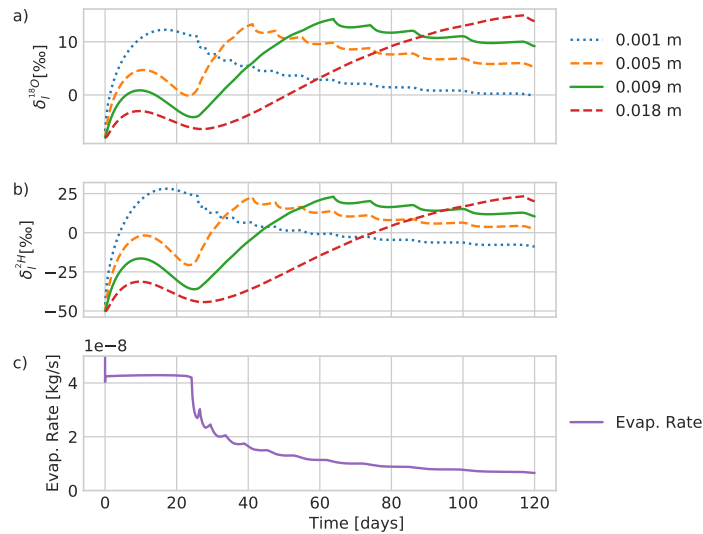


Figure 4: Influence of evaporation behaviour on the isotopic fractionation process in different soil column depths over time. (a),(b) Isotopic composition δ_i^z ; (c) evaporation rate over a 120 day period.

280 During stage-I evaporation, the isotopologues first enrich due to their lower vapor
 281 pressure relative to ordinary water. As the soil begins to dry, the isotopic composition
 282 decreases as isotopologue-depleted air from the atmosphere intrudes into the drying soil.
 283 At a certain state of drying the porous medium reaches the residual saturation. With
 284 no mobile liquid water at the surface, further evaporation is limited by vapor transport
 285 in the gas phase. Compared to before, isotopic species are enriching again, leading to
 286 a second peak. In this stage, the intrusion of air from the atmosphere is decreasing, as
 287 the air volume in the porous medium does not change very much anymore. However, lighter
 288 water isotopologues are still evaporating from the remaining liquid water, resulting in
 289 an increase in the isotopic composition. This leads to the second peak, the "stage-II peak".
 290 When drying further, eventually the water saturation reaches zero and the isotopologue
 291 composition decreases again.

292 These peaks in isotopologue composition are also described in various other mod-
 293 eling studies, e.g. for unsaturated soils by Barnes and Allison (1983). In their study they
 294 consider a soil with a dry layer on top, that is dominated by vapor transport. This de-
 295 scribed peak corresponds to our "stage-II peak" mentioned in this work.

296 In Figure 4, we show that the isotopic composition over time for various depths can
 297 be used to gain further insights into the evaporation and isotopologue transport processes.
 298 In the first soil layer, we only observe a stage-I peak. As this cell is located at the in-
 299 terface, the cell directly dries out when the atmospheric demand can no longer be sup-
 300 plied. In the other depths, the impact of the transition between stage-I and stage-II evap-
 301 oration becomes more visible. However, with increasing soil depths, the evolution of the
 302 stage-I peak becomes less dominant as soils further from the surface are less impacted
 303 by the atmospheric evaporation demand.

304 4.2 Study of fractionation process

305 Mathieu and Bariac (1996) proposed a qualitative study to validate the isotopic
 306 enrichment of their isotope transport model. The aim of this study was to check on the
 307 influencing fractionation parameters by isolating each specific parameter. In Table 2, the
 308 isolated parameters used in the model for this processes study are summarized. Note that
 309 all parameters are listed given a temperature of 289K.

Table 2: Parameter change for fractionation process study

Case	Description	Gas pressure p^i	Gas diffusion coeff. $D_g^{i,air}$	Liq. diffusion coeff. $D_l^{H_2O,i}$	Mole fraction in Ω_{ff}
1	No fractionation	p^{H_2O}	$D_g^{H_2O,air}$	$D_l^{H_2O,self}$	$x_{g,ff}^i = x_{g,pm}^i$
2	Only equilibrium fractionation	p^i	$D_g^{H_2O,air}$	$D_l^{H_2O,self}$	$x_{g,ff}^i = x_{g,pm}^i$
3	Only kinetic fractionation	p^{H_2O}	$D_g^{i,air}$	$D_l^{H_2O,self}$	$x_{g,ff}^i = x_{g,pm}^i$
4	Surface depletion	p^{H_2O}	$D_g^{H_2O,air}$	$D_l^{H_2O,self}$	$x_{g,ff}^i < x_{g,pm}^i$
5	Only liquid diffusion	p^{H_2O}	$D_g^{H_2O,air}$	$D_l^{H_2O,i}$	$x_{g,ff}^i = x_{g,pm}^i$
6	Reference	p^i	$D_g^{i,air}$	$D_l^{H_2O,i}$	$x_{g,ff}^i < x_{g,pm}^i$

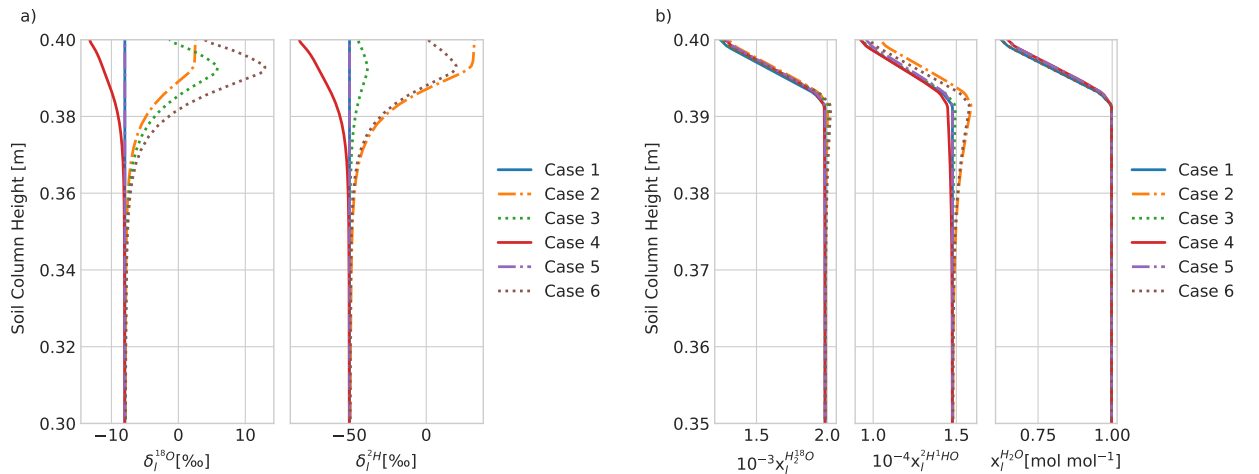


Figure 5: Process behaviour of isolated fractionation parameter at 50 days. (a) Isotopic composition δ_i^j ; (b) mole fraction x_i^k of ordinary water and its isotopes.

310 In Figure 5 the results of our fractionation study are displayed. The fractionation
 311 process is analyzed for the vertical isotope profiles for ${}^2H^1HO$ and $H_2^{18}O$. The study
 312 cases are performed with the same model setup as described in Section 3, and with the
 313 same drying conditions ($v_x = 0.1$ m/s, 50 day period). Additionally, we compare the iso-
 314 tope profiles with the mole fractions of water and its isotopologues in the liquid phase
 315 to enhance our understanding of fractionation processes. It can be seen that the frac-
 316 tionation process is not as obvious in the mole fraction formulation as in the delta nota-
 317 tion.

- 318 • **Case 1 - No isotopic fractionation:** All factors which lead to isotopic fractiona-
 319 tion (vapor pressure difference, liquid and gaseous diffusion coefficients, isotopic
 320 composition gradient between free-flow and porous-medium domain) are neutral-
 321 ized. Hence, no significant fractionation compared to the initial state are obtained
 322 (max. deviation for $H_2^{18}O < 0.199\%$ and for ${}^2H^1HO < 0.030\%$). As we are ob-
 323 serving an evaporation process, a concentration gradient towards the soil surface
 324 is formed (vapor zone). However, as water and its isotopes are both evaporating
 325 with the same slope, the isotopic composition remains constant.
- 326 • **Case 2 - Only equilibrium fractionation:** The equilibrium fractionation fac-
 327 tor describes the tendency of a component to separate from a mixture. In our case,
 328 ${}^2H^1HO$ is more likely to partition from ordinary water than $H_2^{18}O$ ($\alpha_{eq}^{2H^1HO} =$
 329 0.921 , $\alpha_{eq}^{H_2^{18}O} = 0.990$).
 330 By enabling the difference in vapour pressure of the isotopes, the equilibrium frac-
 331 tionation is reintroduced ($p_g^{H_2O} = 1801.4Pa$, $p_g^{2H^1HO} = 1659.88Pa$, $p_g^{H_2^{18}O} =$
 332 $1782.51Pa$). The isotopologues enrich towards the evaporation front due to phase
 333 equilibrium conditions. In the vapour zone the composition remains constant since
 334 the domain has switch into a one-phase system. Thus no equilibrium fractiona-
 335 tion due to phase changes occurs in this zone.
- 336 • **Case 3: Only kinetic fractionation** Compared to Case 1, the binary gas dif-
 337 fusion coefficient is reintroduced for the isotopologues ($D_g^{H_2O,air} = 2.36e^{-5}m^2s^{-1}$,
 338 $D_g^{2H^1HO,air} = 2.30e^{-5}m^2s^{-1}$, $D_g^{H_2^{18}O,air} = 2.29e^{-5}m^2s^{-1}$). Enabling the gas
 339 diffusion coefficient leads to an increase in the unsaturated zone as the isotopo-
 340 logues diffuse slower due to the lower diffusion coefficient, and subsequently to an
 341 decrease in the gaseous zone towards the isotopic-depleted free-flow concentration.
- 342 • **Case 4 - Only surface depletion:** Here, the influence of the depleted atmospheric
 343 conditions ($\delta_g^{2H} = -100$ ‰, $\delta_g^{18O} = -16$ ‰) are analyzed. As drying proceeds,
 344 the isotopic concentration within the porous medium tends to the isotopic con-
 345 centration in free flow.
- 346 • **Case 5 - Only liquid diffusion coefficient:**
 347 The liquid diffusion coefficient of the isotopologues is proportional to the self dif-
 348 fusion coefficient of pure water ($D_l^{H_2O,i} = a^i D_{H_2O,self}^l$)(Mathieu & Bariac, 1996).
 349 As the liquid diffusion may influence the mixing behavior of the isotopologues in
 350 the saturated and unsaturated zone, we isolate the liquid diffusion coefficient in-
 351 stead of only using the self-diffusion coefficient of water for the isotopic species ($D_l^{H_2O,self} =$
 352 $1.819e^{-9}m^2s^{-1}$, $D_l^{2H^1HO} = 1.789e^{-9}m^2s^{-1}$, $D_l^{H_2^{18}O} = 1.759e^{-9}m^2s^{-1}$). The
 353 liquid diffusion coefficient itself does not majorly affect the fractionation process
 354 as the advective term dominates the mixing and flow process in this case (com-
 355 pared to the initial state max. deviation for $H_2^{18}O < 0.122$ ‰ and for ${}^2H^1HO$
 356 $< 0.019\%$).
- 357 • **Case 6 - Reference:** As a reference, we enable all factors leading to fractiona-
 358 tion. The results show both, a high enrichment towards the evaporation front (as
 359 in Case 2) and a depletion towards the soil surface (Case 3 + 4).

360

4.3 Variation of free-flow domain model

361

362

363

364

365

366

367

368

369

In the previous sections, investigations have been focused to laminar flow problems. However, when considering realistic atmospheric conditions with higher wind velocities, turbulent flow conditions must be regarded as well. As stated above, many studies have been focused on integrating turbulent mixing into the isotopic fractionation process by adapting the kinetic fractionation factor (e.g. Quade et al., 2018). By changing our free flow - porous medium coupled transport model by using the Reynold's averaged Navier-Stokes (RANS) equations and choosing a $k-\omega$ -model turbulence model as described in Section 2 and in (Heck et al., 2020; Coltman et al., 2020), we can affect the kinetic fractionation process at the interface region.

370

371

372

373

374

375

376

377

378

379

380

381

382

The velocity profile in the free-flow domain evolves from left to right from a block velocity profile to a fully developed flow profile for turbulent flow. For the laminar cases, a parabolic velocity profile is set on the left side, and from that, the flow profile develops. In Figure 6 the different flow scenarios are schematically displayed. The different flow scenario affect the diffusive flux near the interface, which further influence the evaporation rate at the soil surface (Figure 7) and so the isotopic fractionation behaviour inside the porous medium (Figure 8). As we want to show the variety of our free-flow model, we chose realistic flow scenarios for our laminar and turbulent flow cases. Since laminar flow mostly occurs indoors or under controlled conditions the boundary conditions for the laminar case resemble a wind tunnel. As the isotopic fractionation is an environmental issue, we are also interested in outdoor conditions. Therefore, we choose for the turbulent case boundary conditions which are suitable to replicate outdoor conditions, without a closed top at the upper boundary.

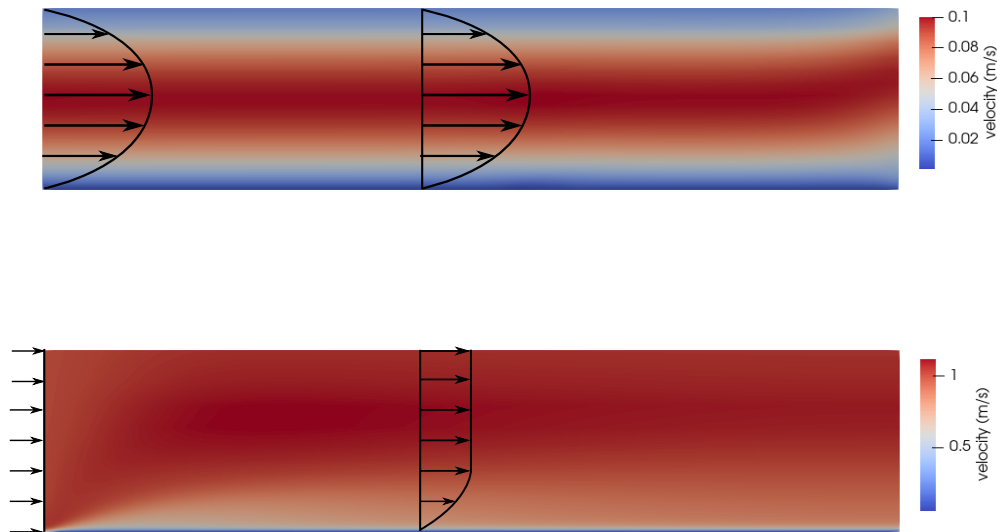


Figure 6: Influence of the boundary layer thickness developed by (a) laminar, (b) turbulent flow on mass transfer at the interface. We assume that the mass transfer is limited at the interface region, boundary layers form based on the present flow type and that outside the formed boundary layer the flow is fully mixed.

383

384

385

For our analysis of the influence of different flow conditions on fractionation processes, we test different free-flow velocities (Table 3). The turbulent flow problems result in different evaporation rates and evaporation profiles (Figure 7), as the maximum

386 evaporation rate is higher and the duration of stage-I is shortened by increasing the flow
 387 velocity.

Table 3: Turbulence parameter. (For parabolic flow profiles, the characteristic length of the Reynolds number (Re_D) is the diameter of the wind tunnel ($d=0.25\text{m}$) and for initial block profile flow (Re_L), we use the length between the starting point of the free-flow domain and the porous-medium domain ($l = 0.6 \text{ m}$.)

Case	Conditions	Flow Velocity [ms^{-1}]	Reynolds Number [-]
1	Laminar	0.1	$Re_D = 1\ 678$
2	Laminar	0.13	$Re_D = 2\ 181$
3	Turbulent	0.5	$Re_L = 2.01\text{e}4$
4	Turbulent	1.0	$Re_L = 4.03\text{e}4$
5	Turbulent	3.0	$Re_L = 1.21\text{e}5$

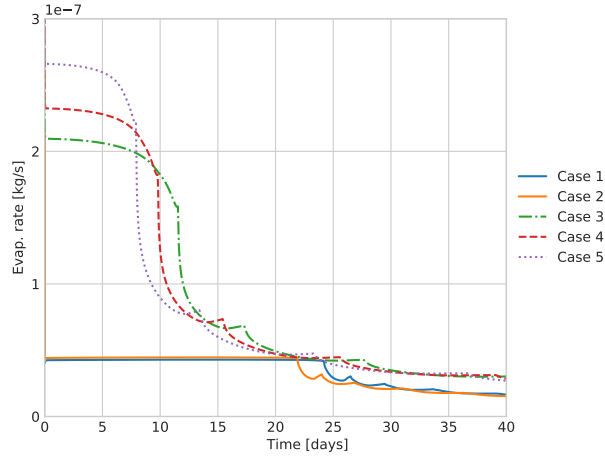


Figure 7: Evaporation rates over time for turbulent (dashed) and laminar (straight) flow problems

388 In the previous section, we hypothesized that the stage of evaporation (stage-I/stage-
 389 II) will have a crucial influence on the isotopic fractionation behavior in the porous medium.
 390 Thus, we analyze the isotopic distribution (in the vertical and horizontal direction) dur-
 391 ing different evaporation states and for different velocities (Figure 8). We compare the
 392 different flow cases among each other during stage-I and stage-II and for the transition
 393 zone between those stages. With this in mind, simulation times are selected such that
 394 all cases reached similar evaporation stages. However, due to the great difference in evap-
 395 oration rates, it is not possible to separate the stages for all cases completely.

396 Vertical isotopic distribution

- 397 • **Stage-I Evaporation:** In this stage, the isotopic fractionation is characterized
 398 by equilibrium fractionation. Whereas the turbulent and laminar flow problems
 399 behave very similarly, laminar cases enrich less towards the soil surface, but show

a greater difference in isotopic composition and a higher isotopic gradient. This is due to the higher evaporation rates seen in the turbulent cases. Thus the influence of the equilibrium fractionation is reduced and therefore less difference in the isotopic composition. However, some differences are still visible; The highest velocities lead to the highest enrichment. A reason for this is the different temperatures during stage-I evaporation. Higher evaporation rates lead to substantial evaporative cooling. The equilibrium fractionation process is very temperature sensitive and lower temperatures lead to lower equilibrium fractionation factors which means more partitioning of the isotopologues.

- **Transition:** A mixed representation of different evaporation states is visible at this point in the simulation. Where the laminar cases are still in stage-I evaporation, the turbulent cases are in different stages of the transition into stage-II evaporation. Thus, the interpretation of the turbulence impact on the isotopic composition in this zone is not absolute, but we regard one representative time. However, in all three turbulent cases, we observe that near the soil surface (0.39-0.38 m) the peak in isotopic composition has decreased in comparison with stage-I evaporation.

While in the transition zone, the soil temperature raises again due to lower evaporation rates and less evaporative cooling. Then the equilibrium fractionation does not affect the isotopic composition that much anymore and kinetic fractionation becomes more dominant.

Since the laminar cases are still in stage-I evaporation, the isotopic fractionation behavior remains similar to the previous stage. However, one may notice that the surface isotopic composition is increased as was observed in the turbulent cases (see Figure 8a). The wind velocities affect the speed of enrichment at the soil surface and the drying of the porous medium but does not significantly affect the maximum isotopic composition at the surface.

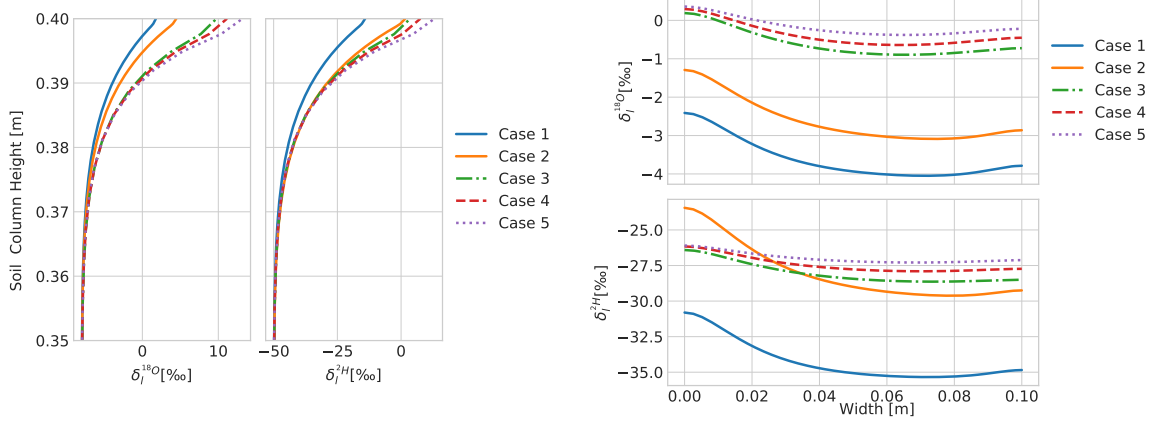
- **Stage-II Evaporation:** Here, all cases are in stage-II evaporation and all cases has developed the characteristic peak of the isotopologues. The turbulent cases show a very similar behaviour. Only minor deviations in the maximal enrichment are visible. For laminar flow, we observe that the maximum enrichment is greater for higher wind velocities, while the evaporation front is nearly on the same level. Still, higher wind velocities lead to drier soil, which in turn effects the peak in isotopic composition.

Horizontal isotopic distribution

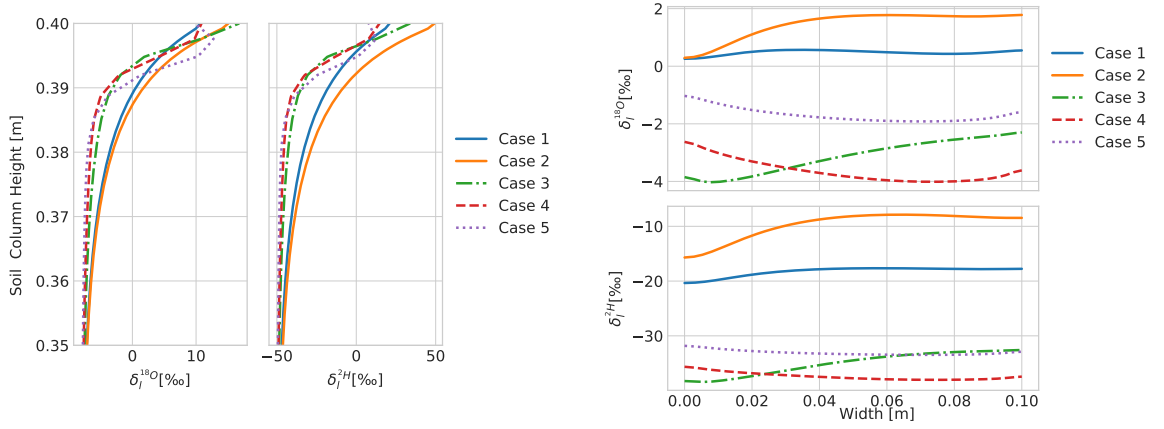
The impact of the varied free-flow conditions and the subsurface thermal boundary conditions can be observed by evaluating the spatial distribution of the isotopic composition at different depths parallel to the interface.

The influence of the different wind velocities is visible in terms of the evolution of isotopic composition. As observed in the vertical profiles, the enrichment in the turbulent cases proceeds faster than the laminar cases. Again, the influence of the different evaporation stages of the different flow problems is visible. In stage-I and stage-II the isotopic composition increases, whereas the isotopic composition is decreasing in the transition zone. During stage-I and stage-II the isotopic composition of the turbulent cases show only minor deviations in comparison with the laminar cases. While in the transition zone, in which the evaporation state may varies for each case, the spatial distribution of the turbulent cases is also varying considerably. Here, the spatial isotopic composition of a developed evaporation front (Case 5), a forming evaporation front (Case 4), and a surface evaporation front (Case 3) are displayed. Further, the effects of decreasing evaporation rates and less evaporative cooling on the horizontal distribution of the isotopic composition during different evaporation steps can be observed here.

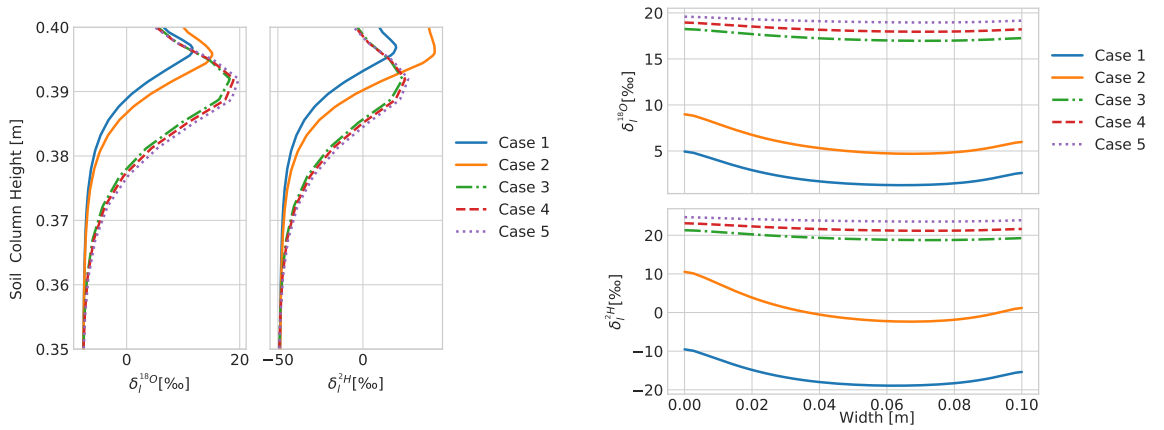
451 Considering the spatial variation of the isotopic enrichment within the single cases,
452 the one-dimensional assumption is for most cases sufficient. In addition, the applied con-
453 duction boundary condition in the porous medium of our virtual case has also a crucial
454 impact on the enrichment of the isotopologues. For special cases, as observed in our lam-
455 inar cases, a larger change in isotopic composition is possible along the horizontal axis.



(a) Stage-I evaporation (t=2 days)



(b) Transition evaporation (t=10 days)



(c) Stage-II evaporation (t=35 days)

Figure 8: Spatial isotopic composition in porous-medium domain for different flow problems (Laminar: Case 1,2 (solid lines); Turbulent: Case 3,4,5 (dashed lines)). Shown are vertical ($x = 0.05$ m) and horizontal ($y = 0.39$ m) isotopic profiles for different evaporation states.

5 Conclusion and Outlook

With the coupled model concept presented in this work, the transport and fractionation of stable water isotopologues during soil-water evaporation can be described. We solve transport equations for ordinary water, its isotopologues, and dry air in the porous medium and the free flow and use suitable coupling conditions to describe the mass, momentum, and energy conservation between the domains. In contrast to other existing models, further parameterization of the kinetic fractionation is not necessary as the transport and mixing in the system is modelled directly.

Considering laminar conditions, it is shown that the coupled model can reproduce the characteristic enrichment peaks in isotopic composition during the evolution of the evaporation front, as well as the depletion of isotopologues in the dry soil during the drying of the soil. Further, a correlation between the isotopic composition and the different stages of evaporation can be observed. In the isotopic composition at certain levels the impact of the different stages of evaporation is visible as during stage-I a first peak in the isotopic composition is observed and a second peak appears in stage-II evaporation. In an additional study, we test the robustness of our model by separating the processes of equilibrium and kinetic fractionation. The effect of wind velocity and turbulent mixing on the isotopic composition in soil is studied. For that, we use a RANS approach for the description of the turbulent flow in the free-flow. This analysis allows us to further study the influence of the evaporation rate and the evaporation stages on the isotopic composition. The temperature-sensitive equilibrium fractionation is affected by higher evaporation rates as less evaporative cooling leads to a higher partitioning of isotopologues. In stage-II evaporation, where the kinetic fractionation is more dominant, we observe a variation in the isotopic compositions of the different flow conditions: The turbulent flow cases have similar characteristic peaks in the isotopic composition, but the laminar flow cases show a greater influence of the wind velocity on the isotopic transport. The analysis in this work has shown that the coupled transport model can be used as a supportive tool to further specify the parametrization of kinetic fractionation.

Besides wind velocity and turbulent mixing in the free flow, other free-flow properties such as radiation and surface topology have a crucial impact on the fractionation in soils and at the soil-atmosphere interface. In (Heck et al., 2020) and (Coltman et al., 2020) it is presented how radiation and surface topology can be implemented in similar transport models. Additionally, the presence of salt concentration in soil waters affects the evaporation rate and so the fractionation process (Sofer & Gat, 1975), as salt precipitation and concentration instabilities occur during the evaporation process in the porous medium (Shokri-Kuehni et al., 2020). The effect of salinity on the fractionation process could be further investigated in the context of this model.

6 Open Research

All code relevant to obtaining the numerical examples is implemented in DuMux (Koch et al., 2021) and can be found under Gitlab (git.iws.uni-stuttgart.de/dumux-pub/Kiemle2022a).

Acknowledgments

We thank the Deutsche Forschungsgemeinschaft (DFG, German Research Foundation) for supporting this work by funding SFB 1313, Project Number 327154368 and the DFG Research Group Satin 2531/14-1. We also thank the DFG for supporting this work by funding SimTech via Germany's Excellence Strategy (EXC 2075 – 390740016).

References

Aleinov, I., & Schmidt, G. (2006). Water isotopes in the GISS modelE land surface

- 503 scheme. *Global and Planetary Change*, 51, 108-120. doi: 10.1016/j.gloplacha
 504 .2005.12.010
- 505 Barnes, C., & Allison, G. (1983). The distribution of deuterium and 18O in dry soils:
 506 1. Theory. *Journal of Hydrology*, 60(1-4), 141–156. doi: 10.1016/0022-1694(83)
 507 90018-5
- 508 Barnes, C., & Allison, G. (1984). The distribution of deuterium and 18O in dry soils:
 509 3. Theory for non-isothermal water movement. *Journal of Hydrology*, 74(1-2),
 510 119–135. doi: 10.1016/0022-1694(84)90144-6
- 511 Beavers, G. S., & Joseph, D. D. (1967). Boundary conditions at a natu-
 512 rally permeable wall. *Journal of Fluid Mechanics*, 30(1), 197–207. doi:
 513 10.1017/s0022112067001375
- 514 Braud, I., Bariac, T., Gaudet, J. P., & Vauclin, M. (2005). SiSPAT-Isotope, a cou-
 515 pled heat, water and stable isotope (HDO and H218O) transport model for
 516 bare soil. part I. model description and first verifications. *Journal of Hydrol-
 517 ogy*, 309(1-4), 277–300. doi: 10.1016/j.jhydrol.2004.12.013
- 518 Brutsaert, W. (1975). The roughness length for water vapor sensible heat, and other
 519 scalars. *Journal of Atmospheric Sciences*, 32(10), 2028 - 2031. doi: 10.1175/
 520 1520-0469(1975)032(2029:TRLFWV)2.0.CO;2
- 521 Coltman, E., Lipp, M., Vescovini, A., & Helmig, R. (2020). Obstacles, inter-
 522 facial forms, and turbulence: A numerical analysis of soil–water evapo-
 523 ration across different interfaces. *Transport in Porous Media*, 134. doi:
 524 10.1007/s11242-020-01445-6
- 525 Craig, H. (1961). Isotopic variations in meteoric waters. *Science*, 133(3465), 1702–
 526 1703. doi: 10.1126/science.133.3465.1702
- 527 Craig, H., & Gordon, L. I. (1965). Deuterium and oxygen 18 variations in the ocean
 528 and marine atmosphere. Consiglio nazionale delle ricerche, Laboratorio de ge-
 529 ologia nucleare Pisa.
- 530 Dongmann, G., Nürnberg, H. W., Förstel, H., & Wagener, K. (1974). On the enrich-
 531 ment of H218O in the leaves of transpiring plants. *Radiation and Environmen-
 532 tal Biophysics*, 11, 41-52. doi: 10.1007/BF01323099
- 533 Fetzer, T., Smits, K. M., & Helmig, R. (2016). Effect of turbulence and roughness
 534 on coupled porous-medium/free-flow exchange processes. *Transport in Porous
 535 Media*, 114(2), 395–424. doi: 10.1007/s11242-016-0654-6
- 536 Flemisch, B., Darcis, M., Erbertseder, K., Faigle, B., Lauser, A., Mosthaf, K., ...
 537 Helmig, R. (2011). DuMux: DUNE for multi-phase,component,scale,physics,...
 538 flow and transport in porous media. *Advances in Water Resources*, 34(9),
 539 1102-1112. (New Computational Methods and Software Tools) doi:
 540 https://doi.org/10.1016/j.advwatres.2011.03.007
- 541 Gat, J. R. (1971). Comments on the stable isotope method in regional groundwa-
 542 ter investigations. *Water Resources Research*, 7(4), 980-993. doi: 10.1029/
 543 WR007i004p00980
- 544 Gonfiantini, R. (1978). Standards for stable isotope measurements in natural com-
 545 pounds. *Nature*, 271(5645), 534-536. doi: 10.1038/271534a0
- 546 Haese, B., Werner, M., & Lohmann, G. (2012). Stable water isotopes in the cou-
 547 pled atmosphere–land surface model echam5-jsbach. *Geoscientific Model Devel-
 548 opment*, 5, 3375-3418. doi: 10.5194/gmd-6-1463-2013
- 549 Haverd, V., & Cuntz, M. (2010). Soil–Litter–Iso: A one-dimensional model for
 550 coupled transport of heat, water and stable isotopes in soil with a litter
 551 layer and root extraction. *Journal of Hydrology*, 388(3-4), 438–455. doi:
 552 10.1016/j.jhydrol.2010.05.029
- 553 Heck, K., Coltman, E., Schneider, J., & Helmig, R. (2020). Influence of radiation on
 554 evaporation rates: A numerical analysis. *Water Resources Research*, 56. doi:
 555 10.1029/2020WR027332
- 556 Horita, J., & Wesolowski, D. (1994). Liquid-vapor fractionation of oxygen
 557 and hydrogen isotopes of water from the freezing to the critical temper-

- ature. *Geochimica et Cosmochimica Acta*, 58(16), 3425–3437. doi: 10.1016/0016-7037(94)90096-5
- IAPWS. (2007). *Revised release on the iapws industrial formulation 1997 for the thermodynamic properties of water and steam* (Tech. Rep. No. IAPWS R7-97(2012)). Lucerne, Switzerland: The International Association for the Properties of Water and Steam.
- Jiang, Z., Xu, T., Mallants, D., Tian, H., & Owen, D. (2018). Numerical modelling of stable isotope (2H and 18O) transport in a hydro-geothermal system: Model development and implementation to the guide basin, china. *Journal of Hydrology*. doi: 10.1016/j.jhydrol.2018.11.065
- Jones, I. P. (1973). Low Reynolds number flow past a porous spherical shell. *Mathematical Proceedings of the Cambridge Philosophical Society*, 73(1), 231–238. doi: 10.1017/S0305004100047642
- Koch, T., Gläser, D., Weishaupt, K., Ackermann, S., Beck, M., Becker, B., . . . Flemisch, B. (2021). DuMux 3 – an open-source simulator for solving flow and transport problems in porous media with a focus on model coupling. *Computers & Mathematics with Applications*, 81, 423–443. (Development and Application of Open-source Software for Problems with Numerical PDEs) doi: 10.1016/j.camwa.2020.02.012
- Kraft, P., Vaché, K., & Breuer, L. (2011). Cmf: A hydrological programming language extension for integrated catchment models. *Environmental Modelling & Software*, 26, 828–830. doi: 10.1016/j.envsoft.2010.12.009
- Kuppel, S., Tetzlaff, D., Maneta, M., & Soulsby, C. (2018). EcH₂O-iso 1.0: Water isotopes and age tracking in a process-based, distributed ecohydrological model. *Geoscientific Model Development*, 11, 3045–3069. doi: 10.5194/gmd-11-3045-2018
- Lehmann, P., Assouline, S., & Or, D. (2008). Characteristic lengths affecting evaporative drying of porous media. *Phys. Rev. E*, 77, 056309. doi: 10.1103/PhysRevE.77.056309
- Luz, B., Barkan, E., Yam, R., & Shemesh, A. (2009). Fractionation of oxygen and hydrogen isotopes in evaporating water. *Geochimica Et Cosmochimica Acta - GEOCHIM COSMOCHIM ACTA*, 73, 6697–6703. doi: 10.1016/j.gca.2009.08.008
- Majoube, M. (1971). Fractionnement en oxygène 18 et en deutérium entre l’eau et sa vapeur. *J. Chim. Phys.*, 68, 1423–1436. doi: 10.1051/jcp/1971681423
- Mathieu, R., & Bariac, T. (1996). An isotopic study (2H and 18O) of water movements in clayey soils under a semiarid climate. *Water Resources Research*, 32(4), 779–789. doi: 10.1029/96WR02995
- Melayah, A., Bruckler, L., & Bariac, T. (1996). Modeling the transport of water stable isotopes in unsaturated soils under natural conditions: 1. theory. *Water Resources Research*, 32, 2047–2054. doi: 10.1029/96WR00674
- Merlivat, L. (1978). Molecular diffusivities of H_2^{16}O , HD^{16}O , and H_2^{18}O in gases. *The Journal of Chemical Physics*, 69(6), 2864–2871. doi: 10.1063/1.436884
- Moore, R. (1937). *Water conduction from shallow water tables*. University of California, Berkeley. doi: 10.3733/hilg.v12n06p383
- Mosthaf, K., Baber, K., Flemisch, B., Helmig, R., Leijnse, A., Rybak, I., & Wohlmuth, B. (2011). A coupling concept for two-phase compositional porous-medium and single-phase compositional free flow. *Water Resources Research*, 47(10). doi: 10.1029/2011wr010685
- Müller, M., Alaoui, A., Kuells, C., Leistert, H., Meusburger, K., Stumpp, C., . . . Alewell, C. (2014). Tracking water pathways in steep hillslopes by $\delta^{18}\text{O}$ depth profiles of soil water. *Journal of Hydrology*, 519, 340–352. doi: 10.1016/j.jhydrol.2014.07.031
- Quade, M., Brüggemann, N., Graf, A., Vanderborght, J., Vereecken, H., & Rothfuss, Y. (2018). Investigation of kinetic isotopic fractionation of water during

- 613 bare soil evaporation. *Water resources research*, 54(9), 6909–6928. doi:
614 10.1029/2018WR023159
- 615 Risi, C., Ogée, J., Bony, S., & Besson, C. (2016). The water isotopic version of the
616 land-surface model orchidee: Implementation, evaluation, sensitivity to hydro-
617 logical parameters. *Journal of Waste Water Treatment & Analysis*, 07. doi:
618 10.4172/2157-7587.1000258
- 619 Rothfuss, Y., Merz, S., Vanderborght, J., Hermes, N., Weuthen, A., Pohlmeier,
620 A., ... Brüggemann, N. (2015). Long-term and high-frequency non-
621 destructive monitoring of water stable isotope profiles in an evaporating soil
622 column. *Hydrology and Earth System Sciences*, 19(10), 4067–4080. doi:
623 10.5194/hessd-12-3893-2015
- 624 Saffman, P. G. (1971). On the boundary condition at the surface of a porous
625 medium. *Studies in Applied Mathematics*, 50(2), 93–101. doi: 10.1002/
626 sapm197150293
- 627 Shokri-Kuehni, S. M. S., Raaijmakers, B., Kurz, T., Or, D., Helmig, R., & Shokri,
628 N. (2020). Water table depth and soil salinization: From pore-scale pro-
629 cesses to field-scale responses. *Water Resources Research*, 56(2). doi:
630 10.1029/2019WR026707
- 631 Shurbaji, A.-R. M., & Phillips, F. M. (1995). A numerical model for the move-
632 ment of H₂O, H₂18O, and 2HHO in the unsaturated zone. *Journal of Hydrol-
633 ogy*, 171, 125-142. doi: 10.1016/0022-1694(94)02604-A
- 634 Sofer, Z., & Gat, J. (1975). The isotope composition of evaporating brines: Effect of
635 the isotopic activity ratio in saline solutions. *Earth and Planetary Science Let-
636 ters*, 26(2), 179-186. doi: 10.1016/0012-821X(75)90085-0
- 637 Somerton, W., Keese, J., & Chu, S. (1974). Thermal Behavior of Unconsolidated Oil
638 Sands. *Society of Petroleum Engineers Journal*, 14(05), 513-521. doi: 10.2118/
639 4506-PA
- 640 Sprenger, M., Leistert, H., Gimbel, K., & Weiler, M. (2016). Illuminating hydro-
641 logical processes at the soil-vegetation-atmosphere interface with water stable
642 isotopes. *Reviews of Geophysics*, 54(3), 674–704. doi: 10.1002/2015rg000515
- 643 Sprenger, M., Tetzlaff, D., Buttle, J., Laudon, H., Leistert, H., Mitchell, C. P.,
644 ... Soulsby, C. (2018). Measuring and modeling stable isotopes of mo-
645 bile and bulk soil water. *Vadose Zone Journal*, 17(1), 170149. doi:
646 10.2136/vzj2017.08.0149
- 647 Stumpp, C., Stichler, W., Kandolf, M., & Simunek, J., Jiri. (2012). Effects of
648 land cover and fertilization method on water flow and solute transport in five
649 lysimeters: A long-term study using stable water isotopes. *Vadose Zone Jour-
650 nal*, 11, 0. doi: 10.2136/vzj2011.0075
- 651 Uhlenbrook, S., Roser, S., & Tilch, N. (2004). Hydrological process representation
652 at the meso-scale: The potential of a distributed, conceptual catchment model.
653 *Journal of Hydrology*, 291, 278-296. doi: 10.1016/j.jhydrol.2003.12.038
- 654 Van Hook, W. A. (1968). Vapor pressures of the isotopic waters and ices. *The Jour-
655 nal of Physical Chemistry*, 72(4), 1234-1244. doi: 10.1021/j100850a028
- 656 Wilcox, D. C. (2008). Formulation of the k-w turbulence model revisited. *AIAA
657 Journal*, 46(11), 2823–2838. doi: 10.2514/1.36541
- 658 Windhorst, D., Kraft, P., Timbe, E., Frede, H.-G., & Breuer, L. (2014). Stable water
659 isotope tracing through hydrological models for disentangling runoff generation
660 processes at the hillslope scale. *Hydrology and Earth System Sciences*, 18,
661 4113-4127. doi: 10.5194/hess-18-4113-2014
- 662 Wong, T., Nusbaumer, J., & Noone, D. (2017). Evaluation of modeled land-
663 atmosphere exchanges with a comprehensive water isotope fractionation
664 scheme in version 4 of the community land model. *Journal of Advances in
665 Modeling Earth Systems*, 9. doi: 10.1002/2016MS000842
- 666 Zhou, T., Simunek, J., Jiri, & Braud, I. (2021). Adapting HYDRUS-1D to
667 simulate the transport of soil water isotopes with evaporation fractiona-

668
669

tion. *Environmental Modelling & Software*, 143, 105118. doi: 10.1016/
j.envsoft.2021.105118